Journal of Materials Chemistry A

PAPER

View Article Online
View Journal | View Issue

Published on 16 September 2014. Downloaded by Monash University on 22/10/2014 23:32:14.

Cite this: J. Mater. Chem. A, 2014, 2, 18791

UV/ozone-assisted low temperature preparation of mesoporous TiO_2 with tunable phase composition and enhanced solar light photocatalytic activity

Xinyi Zhang,*[a] Jianfeng Yao,[b] Muataz Ali,[a] Jing Wei,[b] Huanting Wang,[b] Leslie Y. Yeo,[c] James R. Friend[c] and Douglas R. MacFarlane*[a]

Received 5th August 2014
Accepted 16th September 2014

DOI: 10.1039/c4ta04020a

www.rsc.org/MaterialsA

In this paper, we report a UV/ozone-assisted method for low temperature preparation of mesoporous TiO_2 with controlled crystalline phase. The results showed that the crystallization of mesoporous TiO_2 can occur at temperatures as low as 100 °C under UV/ozone irradiation. Highly crystalline mesoporous anatase TiO_2 was obtained after UV/ozone treatment at 200 °C. The phase transformation from anatase to rutile occurred during the UV/ozone treatment at 300 °C and mesoporous bicrystalline TiO_2 with a controlled mixture of anatase and rutile phases was prepared by adjusting the exposure time. The photocatalytic performance of the mesoporous TiO_2 strongly depends on the crystal structures and the bicrystalline mesoporous TiO_2 exhibits remarkably enhanced solar light photocatalytic activity. This technique can be useful for low temperature preparation of crystalline mesoporous titania on various substrates and may be generalized to the synthesis of other materials.

Introduction

Owing to its superior properties, TiO_2 has been recognized as one of the best materials for realizing photovoltaic and photocatalytic devices.[1–3] TiO_2 nanomaterials with higher photocatalytic efficiency than their bulk phase counterparts have been extensively investigated in photocatalytic reactions.[4–6] The crystallinity and phase of the TiO_2 are crucial for the performance in photocatalysis and devices. In particular, the anatase phase is metastable and has higher photocatalytic activity than the rutile phase. TiO_2 nanoparticles and films with a large quantity in the anatase form and a small quantity in the rutile form therefore exhibit higher photocatalytic activity than their counterparts in pure anatase or rutile forms.[7–9] It has been suggested that this coupling of the anatase and rutile phases allows the transfer of electrons from anatase to rutile TiO_2 as a result of the slightly lower conduction band energy of the rutile phase, thus facilitating the suppression of charge recombination.[7,10,11] Therefore, a direct method to synthesize TiO_2 nanomaterials with control over the phases would be highly desirable for applications in various fields, such as dye-sensitized solar cells.[12–15]

Mesoporous materials through evaporation-induced self-assembly (EISA) have proved to be a valuable alternative to nanoparticles in photovoltaic and photocatalytic applications.[16,17] The advantage of the EISA technique lies in its ability to "tune" the symmetry and properties of the mesostructure by adjusting the composition of the initial solution and the conditions of the sol–gel processes. In addition, the EISA protocols enable the facile generation of robust films on various substrates. So far, mesoporous anatase TiO_2 films have been prepared by using EISA followed by sintering. The main issue with the sintering step, however, is that the high-temperatures required (above 400 °C) not only induce collapse of the pore structure and even the formation of cracks but also limit the choice of substrates to heat-resistant materials.[18] On the other hand, UV/ozone treatment is commonly used in environmental technology, *e.g.*, ozone treatment of water for purification, in the semiconductor industry for cleaning polished flat wafer surfaces, or in organic synthesis for preparing special carbonyl compounds. Whilst UV/ozone has been used for the removal of surfactants from mesostructured silica,[19] to date, the use of UV to induce crystallization on mesoporous materials however has yet to be reported to the best of our knowledge.

In this paper, we therefore show, for the first time, the possibility of fabricating mesoporous TiO_2 by using an UV/ozone-assisted crystallization method. We demonstrate that not only the surfactant can be removed, but highly crystalline mesoporous TiO_2 can also be prepared at low temperatures through UV/ozone treatment. More specifically, we show the direct fabrication of mesoporous TiO_2 with controlled phases from mesoporous anatase TiO_2 to bicrystalline TiO_2 with a

[a]School of Chemistry, Monash University, Melbourne Centre for Nanofabrication, Clayton, VIC3800, Australia. E-mail: xinyi.zhang@monash.edu; douglas.macfarlane@monash.edu

[b]Department of Chemical Engineering, Monash University, Clayton, VIC3800, Australia

[c]Micro/Nanophysics Research Laboratory, RMIT University, Melbourne, VIC 3000, Australia

Published on 16 September 2014. Downloaded by Monash University on 22/10/2014 23:32:14.

controlled mixture of anatase and rutile phases at 300 °C. Furthermore, the sunlight-driven photocatalytic activity of the mesoporous TiO_2 has been investigated and the results show that the photocatalytic performance of the mesoporous TiO_2 increases with the temperature and the bicrystalline mesoporous TiO_2 exhibits the highest photocatalytic activity.

Experimental

Mesoporous TiO_2 samples were synthesized by using a mixture of poly(ethylene oxide)-*b*-poly(propylene oxide)-*b*-poly(ethylene oxide) copolymer (P123), ethanol, concentrated HCl, and tetrabutyl titanate (TBT).[20,21] The mass ratio of P123/TBT/EtOH/HCl was 1 : 2.8 : 30 : 1.8. For a typical synthesis, 1.0 g of P123 was dissolved in 30 g of ethanol, and then 1.8 g of concentrated HCl was slowly added under agitation. 2.8 g of TBT was then added, and the solution was stirred for 4 h. The resulting solutions were transferred into Petri dishes and subsequently sealed and aged at room temperature for 2 weeks. The dry gel films were subsequently treated using a benchtop UV/ozone cleaning system (SAMCO UV-1, Sunnyvale, CA). The as-prepared TiO_2 films of about 150 mg and 1 mm thick were treated by UV and UV/ozone at different temperatures for 4 h unless otherwise advised. All chemical reagents used in this study were of analytical grade and were supplied by Sigma-Aldrich (Australia).

Nitrogen adsorption–desorption experiments were performed using an ASAP 2020MC analyzer (Micromeritics, Norcross, GA). The samples were added into the sample tube and degassed at 200 °C for 6 h prior to measurement. The mass of the samples was recorded by subtracting the mass of the empty sample tube before degassing from the mass of the sample tube plus the sample after degassing. The N_2 sorption isotherms were obtained in liquid nitrogen at 77 K. The Brunauer–Emmett–Teller (BET) method was utilized to calculate the specific surface area. The total pore volume was estimated from the adsorbed amount at a P/P_0 value of 0.995. The pore size distribution was calculated from the desorption branch of the isotherm by using the Barrett–Joyner–Halenda (BJH) method. The morphology and microstructure of the mesoporous TiO_2 films were investigated using a Philips PW1140/90, an X-ray diffractometer (XRD) with CuKα radiation (25 mA and 40 kV), a Vertex 70 Fourier-transform infrared spectrophotometer (FTIR, Bruker) and a transmission electron microscope (TEM, JEOL-2011). The concentrations of the dye solutions were 50 mg l^{-1} 10 mg of the mesoporous TiO_2 samples were added into 20 ml dye solution and the muddy solution was dispersed using an ultrasonic instrument for 30 min, and then irradiated by using a solar simulator (AM 1.5) with a power of 100 mW cm^{-2} at room temperature and the light intensity was 1 sun. After the photocatalytic experiment, the remaining dye solutions were collected and analyzed. A UV-240 ultraviolet-visible spectrometer was used to record the change of the absorbance of the dye solution.

Results and discussion

Fig. 1 shows the XRD spectra of the obtained mesoporous TiO_2 samples. It can be seen that the UV has a remarkable influence

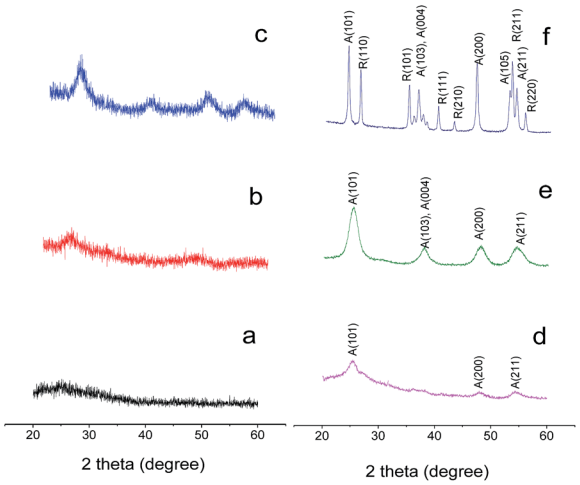

Fig. 1 XRD spectra of mesoporous TiO_2 after treatment at different temperatures without (a–c) and with UV/ozone treatment (d–f) for 4 h: (a and d) 100 °C, (b and e) 200 °C, and (c and f) 300 °C.

on the crystallinity of the mesoporous TiO_2. The (101) peaks of anatase appeared after the UV/ozone treatment at 100 °C, while only broad peaks are obtained at 100 °C without UV/ozone irradiation. The crystallinity of the mesoporous TiO_2 films is seen to increase with the increase in temperature. Highly crystalline TiO_2 was obtained after 4 h of UV treatment at 200 °C, while broad humps are observed at 200 °C in the absence of UV/ozone treatment. The phase transformation from the anatase to rutile form occurred by increasing the temperature, and highly crystalline mesoporous TiO_2 comprising a mixture of anatase and rutile forms was obtained after 4 h of exposure at 300 °C. The amount of anatase and rutile phases in the TiO_2 samples was analysed by taking the ratio of the two most intense peaks of the anatase I_A (101) and rutile I_R (110).[22] The fraction of the rutile phase in the TiO_2 samples was observed to increase with the increase of exposure time, which reached about 45 wt% after 4 h of exposure at 300 °C.

The mesoporous TiO_2 samples were further investigated by transmission electron microscopy (TEM). The TEM images of the TiO_2 samples after UV/ozone treatment at 200 °C and 300 °C are displayed in Fig. 2. Fig. 2a exhibits the plain view of the mesoporous TiO_2 films, where ordered hexagonally organized mesopores with pore sizes of 3–5 nm can be clearly observed. Fig. 2c shows the corresponding electron diffraction (ED) pattern and the continuous strong rings can be indexed to the anatase TiO_2 structure. The high-resolution TEM (HRTEM) image is displayed in Fig. 2e wherein the well-recognized lattice spacings of 0.35 and 0.19 nm correspond to the anatase (101) and (200) atomic planes, respectively. Fig. 2b shows the TEM image of the plain view of the mesoporous TiO_2 after 4 h of treatment at 300 °C, where the assembly of nanoparticles with sizes ranging from 5 to 8 nm can be observed. Fig. 2d shows the corresponding electron diffraction (ED) pattern and the continuous strong rings correspond to the anatase TiO_2 structure. But rutile phases are also clearly visible. The HRTEM image of the mesopore wall in the mesoporous TiO_2 is displayed

 This journal is © The Royal Society of Chemistry 2014

Published on 16 September 2014. Downloaded by Monash University on 22/10/2014 23:32:14.

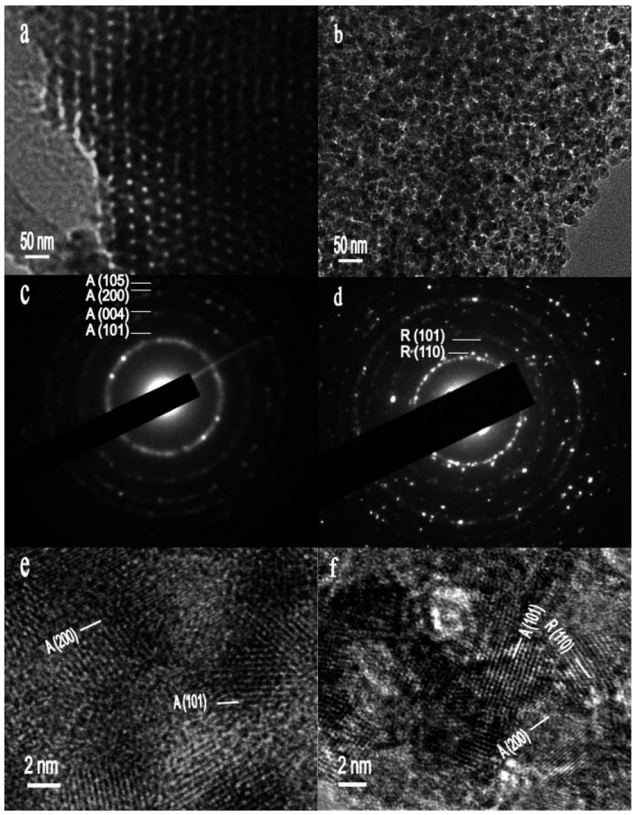

Fig. 2 TEM images of mesoporous TiO_2 and the corresponding electron diffraction patterns as well as HRTEM images after UV/ozone treatment for 4 h at 200 °C (a, c and e) and 300 °C (b, d and f), respectively.

in Fig. 2f, where clear anatase (101) and (200) and rutile (110) atomic planes with respective spacings of 0.35 and 0.19 nm and 0.32 nm are visible. The ED patterns are in accordance with the XRD analysis. The N_2 sorption isotherms of the mesoporous TiO_2 show type-IV curves with clear condensation steps, indicating uniform mesopores (Fig. 3a). The BET surface areas of TiO_2 samples are calculated from nitrogen sorption results to be 105.2 and 123.5 $m^2\ g^{-1}$ for the TiO_2 sample prepared at 200 °C and 300 °C respectively. The pore size distribution curves (Fig. 3b), calculated by the BJH method based on the desorption branch, show that the TiO_2 samples have a very clear mesoporous structure with pore size centred at 5.4 and 7.9 nm after UV/ozone treatment at 200 °C and 300 °C, respectively.

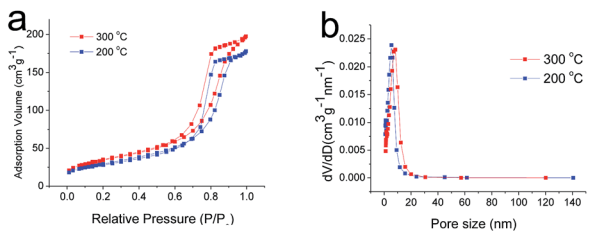

Fig. 3 (a) N_2 sorption isotherm and (b) the pore size distribution curves of mesoporous TiO_2 after UV/ozone treatment for 4 h at 200 °C and 300 °C, respectively.

The FT-IR spectra of the TiO_2 samples treated under UV/ozone irradiation at different temperatures are shown in Fig. 4. The strong infrared absorption bands at around 2850–2930 and 1100 cm^{-1} can be observed for the as-prepared sample (Fig. 4a), corresponding to the C–H and C–O–C stretching vibration of P123, respectively.[23,24] They however become weak and subsequently disappear as the temperature is increased. The higher the temperature, the shorter the time required for the removal of surfactants; the surfactants were removed after UV/ozone treatment at 200 °C for 4 h. The bands in the range of 400–1000 cm^{-1} can be attributed to the vibrations of Ti–O.[25,26] The adsorption band of Ti–O appeared after UV/ozone treatment at 100 °C (Fig. 4b). These bands became sharper with an increase in the temperature, with two sharp bands appearing at 200 °C and 300 °C, further confirming the crystallization of mesoporous TiO_2 (Fig. 4c and d). For comparison, the as-prepared TiO_2 was treated at 200 °C under UV irradiation in the absence of ozone. Fig. 5a shows the FT-IR spectrum of the TiO_2 sample. It can be seen that the C–H and C–O–C stretching vibration of P123 as well as the adsorption band of Ti–O are clearly visible, suggesting that the crystallization of TiO_2 occurred under the UV irradiation without the removal of the surfactant. The XRD spectrum further confirms the formation of anatase TiO_2 (Fig. 5b).

UV irradiation has long been used for photo-induced polymerization in which the energy absorption and transfer lead to the subsequent polymerization of the sample, in a manner similar to that in thermal polymerization. However, the present study is the first demonstration of UV-induced crystallization of mesoporous materials. As a rigorous explanation for the underlying mechanism of UV-induced crystallization has yet to be proposed, we offer a speculative explanation here. Since in our case, tetrabutyl titanate is hydrolyzed and condensed, and an amorphous TiO_2 network is formed after the sol–gel process, it is possible that UV absorption by these materials could result in the production of several forms of localised energetic excitation, for example, bond cleavage, electronic excitation or heat. Photothermal heating of a sample generally produces a temperature rise. For example, it has been reported that UV irradiation could increase the temperature of gel TiO_2 films by less than 40 K.[27] Such an increase in temperature should however not be able to induce crystallization of the TiO_2 film at room temperature. Another possibility lies in the electronic

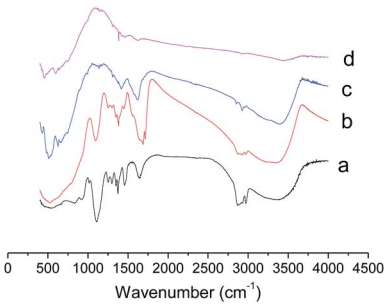

Fig. 4 FT-IR spectra of mesoporous TiO_2 treated under UV/ozone treatment for 4 h: (a) as-prepared; (b) 100 °C; (c) 200 °C; and (d) 300 °C.

Published on 16 September 2014. Downloaded by Monash University on 22/10/2014 23:32:14.

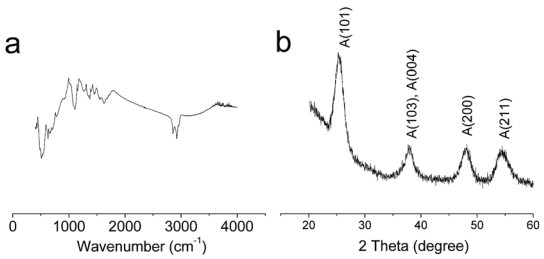

Fig. 5 (a) FT-IR spectrum and (b) XRD spectrum of TiO_2 after UV irradiation without ozone at 200 °C for 4 h.

excitation induced by UV irradiation. UV photons can directly induce dehydration and bond cleavage through electronic excitation, which depend on the incident photon density and the photo-sensitivity of the chemical bonds in the samples. Considerable structural rearrangement inducing nucleation and phase formation is then possible under certain conditions. For instance, UV laser-induced crystallization of sol–gel-derived indium oxide films has been previously reported, in which it was proposed that electronic excitation in the disordered structure of sol–gel-derived films was responsible for the crystallization.[28] Our results support this proposition. It is likely that the crystallization of mesoporous TiO_2 is a consequence of the synergetic effect between the photon energies arising from both UV irradiation and thermal effects, as we shall verify below.

We note that thermally driven bulk phase transformation from anatase to rutile only occurs under high temperatures (above 600 °C) in the absence of UV irradiation.[29] However, the phase transformation of TiO_2 nanoparticles can be achieved at relatively low temperatures (465 °C)[30] or by light irradiation.[31] For example, light irradiation is able to induce an athermal anatase-to-rutile phase transition on TiO_2 nanoparticles and that the mechanism underlying the phase transition is attributed to intragap irradiation.[31] As shown in Fig. 6, the rutile phase appeared in our experiments after UV/ozone treatment at 300 °C for 1 h, but no rutile phase was observed after UV/ozone treatment at 200 °C for 6 h. As such, it is therefore reasonable to conclude that both UV and thermal components contribute to the formation of the rutile phase in the mesoporous TiO_2 films that were synthesized in the present work. Such photothermal effects lead to the activation of the TiO_2 surface and the nucleation of rutile crystallites. The fraction of the rutile phase in the sample increases remarkably after treatment at 300 °C from 1 h to 4 h, revealing that the rutile phase forms from the anatase phase and that the phase transformation increases with the increase in the exposure time. The fact that the rutile phase was not obtained by thermal annealing the TiO_2 films at 300 °C suggests that bond cleavage occurred as the irradiation promoted the rearrangement of the atomic network, resulting in the formation of the stable rutile phase. The nucleation and growth of the rutile phase then altered the mesostructure of TiO_2, resulting in the bicrystalline TiO_2 nanoparticle film.

The mesoporous TiO_2 samples prepared by UV/ozone treatment at different temperatures for 2 h were characterized by the

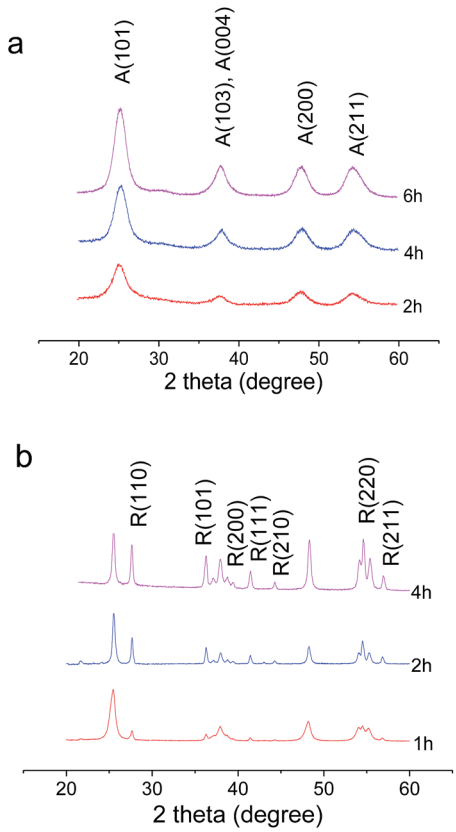

Fig. 6 XRD spectra of mesoporous TiO_2 after UV/ozone treatment at (a) 200 °C and (b) 300 °C with different times.

degradation of Rhodamine B (RB) dye under solarlight irradiation. The same TiO_2 samples without UV/ozone treatment were also investigated for comparison. As shown in Fig. 7, the photocatalytic activity of the mesoporous TiO_2 samples is significantly increased by the UV/ozone treatment, confirming the UV-induced crystallization of the TiO_2 phase. The degradation rate of RB reaches the highest on mesoporous TiO_2 prepared under the UV/ozone treatment at 300 °C. The photocatalytic activity of mesoporous TiO_2 increases with the treatment temperature,

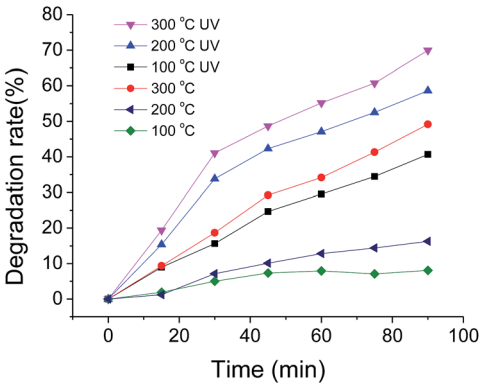

Fig. 7 Photocatalytic degradation of dyes as a function of irradiation time on mesoporous TiO_2 prepared under different temperatures with and without UV/ozone treatment.

This journal is © The Royal Society of Chemistry 2014

Published on 16 September 2014. Downloaded by Monash University on 22/10/2014 23:32:14.

revealing that the crystallinity and phase of mesoporous TiO_2 are critical for dye degradation. The mesoporous TiO_2 sample obtained at 300 °C exhibits higher activity than other literature samples.[32–34] The synergistic effect between anatase and rutile TiO_2 should contribute to the enhanced activity of mesoporous TiO_2.[35,36] According to the TEM observation, the bicrystalline TiO_2 is composed of nanoparticles. It is expected that the introduction of mesospaces into nanoparticle assemblies combines the best features of TiO_2 mesopores and nanoparticles, hence further enhancing their photocatalytic activities.

Conclusions

In summary, we have developed a UV/ozone-assisted method for low temperature preparation of crystalline mesoporous TiO_2, in which control over the phase and composition was achieved simply by adjusting the temperature. In addition, we have proposed a possible mechanism for this UV-induced crystallization and phase formation. The bicrystalline mesoporous TiO_2 exhibits excellent photocatalytic activities. The preparation method presented here is anticipated to open up a new approach to the fabrication of new photodevices based on crystalline mesoporous semiconductors, such as high-efficiency dye-sensitized solar cells and immobilized catalyst photoreactors.

Acknowledgements

This work was supported by the Australian Research Council (no. DP120104334). D. R. M. thanks the Australian Research Council for the Australian Laureate Fellowship. This work was performed in part at the Melbourne Centre for Nanofabrication (MCN) in the Victorian Node of the Australian National Fabrication Facility (ANFF).

References

1 A. Hagfeldt and M. Grätzel, *Chem. Rev.*, 1995, **95**, 49–68.
2 M. Takeuchi, S. Sakai, A. Ebrahimi, M. Matsuoka and M. Anpo, *Top. Catal.*, 2009, **52**, 1651–1659.
3 T. Inoue, A. Fujishima, S. Konishi and K. Honda, *Nature*, 1979, **277**, 637–638.
4 W. Zhao, Y. L. Sun and F. N. Castellano, *J. Am. Chem. Soc.*, 2008, **130**(38), 12566–12567.
5 X. B. Chen, L. Liu, P. Y. Yu and S. S. Mao, *Science*, 2011, **331**(6018), 746–750.
6 J. K. McCusker, *Science*, 2001, **293**(5535), 1599–1601.
7 Z. Liu, X. Zhang, S. Nishimoto, M. Jin, D. A. Tryk, T. Murakami and A. Fujishima, *Langmuir*, 2007, **23**(22), 10916–10919.
8 R. J. Bickley, T. Gonzalez-Carreno, J. S. Lees, L. Palmisano and R. D. Tilley, *J. Solid State Chem.*, 1991, **92**, 178–190.
9 T. Kawahara, Y. Konishi, H. Tada, N. Tohge, J. Nishii and S. Ito, *Angew. Chem., Int. Ed.*, 2002, **114**, 2935–2937.
10 H. Tang, K. Prasad, R. Sanjines, P. E. Schmid and F. Levy, *J. Appl. Phys.*, 1994, **75**, 2042–2047.
11 T. Kawahara, T. Ozawa, M. Iwasaki, H. Tada and S. Ito, *J. Colloid Interface Sci.*, 2003, **267**, 377–381.
12 U. Bach, D. Lupo, P. Comte, J. E. Moser, F. Weissörtel, J. Salbeck, H. Spreitzer and M. Grätzel, *Nature*, 1998, **395**, 583–585.
13 S. Agarwala, M. Kevin, A. S. W. Wong, C. K. N. Peh, V. Thavasi and G. W. Ho, *ACS Appl. Mater. Interfaces*, 2010, **2**(7), 1844–1850.
14 K. M. Gopal, S. Karthik, P. Maggie, K. V. Oomman and G. A. Craig, *Nano Lett.*, 2006, **6**, 215–218.
15 H. Yoshitake and D. Abe, *Microporous Mesoporous Mater.*, 2009, **119**, 267–275.
16 M. M. Turnbull and C. P. Landee, *Science*, 2002, **298**, 1723–1724.
17 D. Y. Zhao, P. D. Yang, N. Melosh, J. L. Feng, B. F. Chmelka and G. D. Stucky, *Adv. Mater.*, 1998, **10**(16), 1380–1385.
18 S. Y. Choi, M. Mamak, N. Coombs, N. Chopra and G. A. Ozin, *Adv. Funct. Mater.*, 2004, **14**(4), 335–344.
19 M. T. J. Keene, R. Denoyel and P. L. Llewellyn, *Chem. Commun.*, 1998, 2203–2204.
20 H. S. Yun, K. Miyazawa, H. S. Zhou, I. Honma and M. Kuwabara, *Adv. Mater.*, 2001, **13**(18), 1377–1380.
21 K. Hou, B. Z. Tian, F. Y. Li, Z. Q. Bian, D. Y. Zhao and C. H. Huang, *J. Mater. Chem.*, 2005, **15**, 2414–2420.
22 H. Z. Zhang and J. F. Banfield, *J. Phys. Chem. B*, 2000, **104**, 3481–3487.
23 A. Hozumi, Y. Yokogawa, T. Kameyama, K. Hiraku, H. Sugimura, O. Takai and M. Okido, *Adv. Mater.*, 2000, **12**(13), 985–987.
24 J. Q. Wang, J. F. Wang, Q. Sun, W. Wang, Z. Y. Yan, W. J. Gong and L. Min, *J. Mater. Chem.*, 2009, **19**, 6597–6604.
25 J. C. Yu, L. Zhang, Z. Zheng and J. Zhao, *Chem. Mater.*, 2003, **15**, 2280–2286.
26 S. Chu, L. L. Luo, J. C. Yang, F. Kong, S. Luo, Y. Wang and Z. G. Zou, *Appl. Surf. Sci.*, 2012, **258**, 9664–9667.
27 H. Imai, K. Awzu, M. Yasumori, H. Onuki and H. Hirashima, *J. Sol-Gel Sci. Technol.*, 1997, **8**, 365–369.
28 H. Imai, A. Tominaga, H. Hirashima, M. Toki and N. Asakuma, *J. Appl. Phys.*, 1999, **85**, 203–207.
29 H. Zhang and J. F. Banfield, *J. Mater. Chem.*, 1998, **8**, 2073–2076.
30 H. Zhang and J. F. Banfield, *Am. Mineral.*, 1999, **84**, 528–535.
31 P. C. Ricci, C. M. Carbonaro, L. Stagi, M. Salis, A. Casu, S. Enzo and F. Delogu, *J. Phys. Chem. C*, 2013, **117**, 7850–7857.
32 W. J. Sun, J. Li, G. Mele, Z. Q. Zhang and F. X. Zhang, *J. Mol. Catal. A: Chem.*, 2013, **366**, 84–91.
33 J. Yang, C. C. Chen, H. W. Ji, W. H. Ma and J. C. Zhao, *J. Phys. Chem. B*, 2005, **109**, 21900–21907.
34 X. Y. Li, C. G. Hu, X. Wang and Y. Xi, *Appl. Surf. Sci.*, 2012, **258**, 4370–4376.
35 Z. Y. Liu, X. T. Zhang, S. Nishimoto, M. Jin, D. A. Tryk, T. Murakami and A. Fujishima, *Langmuir*, 2007, **23**, 10916–10919.
36 P. G. Smirniotis and B. Sun, *Catal. Today*, 2003, **88**, 49–59.